Ambiguity of applying the Wildermuth-Tang rule to estimate the quasibound states of α particles in α emitters

W. M. Seif [1,2,*] A. M. H. Abdelhady [1] and A. Adel [1,†]

[1]*Department of Physics, Faculty of Science, Cairo University, 12613 Giza, Egypt*

[2]*Beni-Suef University, Faculty of Navigation Science and Space Technology, 62521 Beni-Suef, Egypt*

(Received 28 November 2019; revised manuscript received 30 April 2020; accepted 21 May 2020; published 11 June 2020)

The Wildermuth-Tang (WT) prescription is used to verify the Bohr-Sommerfeld (BS) quantization condition in the α-decay problem. It gives the global quantum number that relates the number of nodes of the quasibound radial wave function of the α-daughter system to the shell model and Pauli exclusion principle. Here we examine the applicability of the WT rule in the α-decay microscopic calculations that start with solving the stationary Schrödinger wave equation for different types of the interaction potentials. We found that applying the BS quantization condition along with the WT prescription for the potentials that have no internal pocket yields a large number of nodes in the radial wave function compared to the potentials characterized with an automatic physical internal pocket, which likely produce nodeless or at most a two-node interior wave function. This gives confidence in the latter type of the potentials that efficaciously simulates the Pauli principle by considering the change in the intrinsic kinetic energy. However, it is possible to reproduce the observed half-life data using the potentials that have no automatic internal pocket with applying the BS quantization condition with quantum numbers which are significantly less than that obtained from the WT rule, upon properly normalizing the potential.

DOI: 10.1103/PhysRevC.101.064305

I. INTRODUCTION

The radioactive emission of an α particle is deemed to be one of the underlying decay channels for heavy and superheavy nuclei [1–6]. The interpretation of this decay mode is a fruitful way to provide substantial information about several crucial problems in modern nuclear structure and nuclear astrophysics such as neutron skin thickness [7,8], shell and pairing effects [9–11], identification of shape staggering [12], stellar nucleosynthesis [13], and synthesis and decay of superheavy elements [3–6,14,15].

Based on fundamental quantum mechanical principles, Gamow [16] and, independently, Gurney and Condon [17] described the α-decay process as a preformed α particle undergoing quantum mechanical tunneling from the decaying nucleus through an impenetrable barrier. Associated with the rapid development of experimental facilities, in the past few decades, α-decay spectra have been measured with improved accuracy [5,18]. The revival of interest in the α decay is attributed to the simplicity of its experimental identification and the wealth of spectroscopic information it provides, which greatly expands our knowledge on several nuclear structure properties [4,19]. The challenge is basically to understand and interpret these experimental data and efficiently formulate correlations between different observables.

Several phenomenological and microscopic models have been developed to describe the α-decay [20] process. These models fall into three broad categories: empirical formulations [21–25], semiclassical approximations [26–28], and microscopic models [29–33]. In the adopted framework of the preformed cluster model, our consideration for the α-decay process is consistent with the last group which involves the numerical solution of Schrödinger equation for quasibound states [30]. The α cluster is assumed to be formed in the parent nucleus with a definite preformation probability. Once it is formed, it keeps on assaulting the Coulomb barrier to tunnel from the nucleus with a certain penetration probability [34]. The penetration probability through the α-daughter potential barrier can be nicely obtained by calculating the ratio of the squared transmitted to the squared incident amplitudes of the wave function [35,36], based on the numerical solution of the time-independent Schrödinger wave equation in the relative separation coordinate.

The present study is based on the exact solution of the relative motion Schrödinger wave equation of the α-daughter system with the implementation of the Bohr-Sommerfeld quantization rule, which requires that the action integral to the system must equal a half-integer times Planck's constant. It guarantees that the obtained quasibound state is correct for the quantization of the energy of a periodic system [27,37]. The eigencharacteristics of the α-cluster quasibound state can be approximately defined by the Wildermuth-Tang (WT) prescription [38], which relates an α cluster to the shell model and accounts for the Pauli exclusion principle [39]. A

*wseif@sci.cu.edu.eg

†ahmedadel@sci.cu.edu.eg

quasibound state of the α cluster orbiting the core is characterized by a global quantum number G, whose values are chosen to ensure that the clusterization of α cluster occurs outside the shell occupied by the core nucleus [30,39]. The value of the global quantum number can be determined in terms of WT rule [30,39].

When the Wildermuth-Tang (WT) rule is applied to verify the Bohr-Sommerfeld quantization condition in the α-decay problem, we face ambiguity when different types of interaction potentials are considered. The WT rule is used to find the global quantum number G, which is related to the number of nodes (n) of the quasibound radial wave function of the α-daughter system [27]. This in turn relates n to the shell model and Pauli exclusion principle [39]. A relatively large number of nodes $n > 2A_C$ was estimated for the calculations based on the nuclear potentials of no repulsive core, such as the folding potential based on the M3Y-type NN forces [26,30,40,41], the proximity potential [42], and the phenomenological Woods-Saxon [37], "cosh" [43], and "universal" [44] forms of the potential, and also the potential barriers extracted from the generalized liquid-drop model [45].

In contrast, when potentials of a repulsive core are considered, the decaying state would be a zero-node ($n = 0$) eigenstate [36,46,47]. This has been interpreted microscopically and semimicroscopically in many decay studies in terms of interaction potentials based on the Skyrme energy-density functional [46], which is specified by a deep internal pocket. The same situation is also microscopically obtained based on folding potential in terms of M3Y NN force, which is improved by a repulsive core due to the change of intrinsic kinetic energy [36] or using a phenomenological repulsive core [47,48]. In this study, we try to find the genuine source of this ambiguity of the value of the quantum number needed to describe the motion of the emitted α particle around the internal pocket of the α-daughter potential.

In this regard, we perform a systematic study of the α-decay process for the ground-state to ground-state favored decay modes of three isotopic chains, namely the even(Z)–even (N) and even-odd radioactive isotopes of tellurium and polonium, and the odd-even and odd-odd isotopes of astatine. We adopt a few potentials of two different types for the α-daughter system. These potentials are normalized by applying the Bohr-Sommerfeld quantization condition, with and without the Wildermuth-Tang (WT) rule. In general, the adopted potentials either have no repulsive core, such as the density-independent M3Y-Paris NN interaction and its density-dependent CDM3Y-230 form, or have a repulsive core, such as the improved folding potential [36] and the potential based on the Skyrme energy-density functional. The potentials with a repulsive core are more realistic than the potentials without a repulsive core. For the potential models with no repulsive core, the effects of the Pauli exclusion principle and the structure forbiddenness on the preformation of the α cluster in the parent nucleus are taken into account by Wildermuth-Tang rule. It is based on the oscillator shell model, which allows the low-energy nucleons to move relatively undisturbed throughout the nuclear volume. Based on the numerical solution of the relative motion Schrödinger wave equation of the α-core system, we extract the eigen wave function for each α-decay process characterized with the Q-value energy. In terms of the calculated penetration probability P, assaulting frequency ν, and the experimental half-life ($T_{1/2}^{\rm exp}$), we extract the preformation probability factor S_α. The preformation probability has a clear dependence on the internal part of the potential, due to the effect of Pauli blocking from the saturated core density that influences the wave function of the quasibound state for the α-core system. Through this study, we clarify the ambiguity of applying the WT rule to describe the α-decay process using the above-mentioned types of potentials for the α-daughter system.

The paper is organized as follows. Section II gives the relevant details of the theoretical framework used to compute the interaction potential, the penetration probability, assaulting frequency, and the preformation probability factor. Section III is devoted to the numerical results and discussions. The conclusions drawn from the present study are given in Sec. IV.

II. THEORETICAL FRAMEWORK

We begin by considering an α cluster interacting with a core nucleus inside the decaying nucleus, through a microscopic potential. The radial $u_\ell(r)$ wave function [$\psi = Y_{\ell m}(\theta,\phi)u_\ell(r)/r$] can be obtained by solving the radial Schrödinger equation for the dinuclear system,

$$-\frac{\hbar^2}{2\mu}\frac{d^2}{dr^2}u_\ell(r)+\left[V_N(r)+V_C(r)+\frac{\ell(\ell+1)\hbar^2}{2\mu r^2}\right]u_\ell(r) = E\,u_\ell(r). \tag{1}$$

The total α-daughter interaction potential, as the sum of the attractive potential (V_N) and the repulsive Coulomb potential (V_C) plus the centrifugal part, is written as [49]

$$V_T(r) = \lambda V_N(r) + V_C(r) + \frac{\hbar^2}{2\mu}\frac{\ell\,(\ell+1)}{r^2}. \tag{2}$$

The Langer modified form of the centrifugal potential, $V_\ell = \frac{\hbar^2}{2\mu}\frac{(\ell+\frac{1}{2})^2}{r^2}$, can be safely used with the potentials that have no repulsive core. In solving the Schrödinger wave equation for quasibound states of the α-core system, a normalization factor λ is introduced to the nuclear potential with its direct and exchange parts to reproduce the quasibound state wave function characterized by the experimental Q value. This factor λ is determined through an approximate rule for the quantization of the energy of a periodic system. This rule is well known as the Bohr-Sommerfeld (BS) quantization condition [37], which fulfills the periodicity of particle motion and ensures that the action integral of the system must equal a half-integer times Planck's constant,

$$\int_{r_1}^{r_2} k(r)\,dr = (2n+1)\frac{\pi}{2}. \tag{3}$$

The wave number is given in terms of the Q value of the decay as $k(r) = \sqrt{2\,\mu\,|V_T(r)-Q|/\hbar^2}$. n defines the number of nodes of the radial quasibound wave function in its internal region [27,30]. $r_{i=1,2,3}$(fm) are the three turning points given by $V_T(r_i) = Q$, i.e., when the total potential is equal to the Q value of the decay.

According to the Pauli exclusion principle, two nucleons cannot occupy the same quantum state, and therefore the nucleons that make up the α cluster have to be placed above the Fermi surface of the core nucleons. That is, the α cluster is formed on the surface of the parent nucleus. This can be approximately satisfied through the Wildermuth-Tang rule [38], which restricts the quantum numbers n (i.e., number of internal nodes) of relative motion to values compatible with an α cluster consisting of nucleons in shell-model orbitals above those already occupied by the core nucleons [30,39]. This condition is given in terms of the global quantum number (G), which relates the number of internal nodes n in the radial wave function and the orbital angular momentum ℓ of the relative motion, as

$$G = 2n + \ell = \sum_{i=1}^{n_c} (2n_i + \ell_i) - \bar{g}. \tag{4}$$

Here n_c gives the number of nucleons forming the cluster. The values of n_i and ℓ_i correspond to the filling the shell-model orbitals above the closed core, and $\bar{g}$ is the number of quanta taken up by the cluster internal motion. This condition is valid for systems in which the core and cluster nucleons move in oscillator potentials with a common oscillator length.

One can find the penetration probability as the ratio between the squared amplitude of transmitted wave function and that of the incident wave function at the beginning of the Coulomb barrier [35],

$$P = \frac{|A(u_\ell(r \gg r_3))|^2}{|A(u_\ell(r_2))|^2}. \tag{5}$$

This expression offers an accurate microscopic method to find the penetration probability directly from the obtained normalized wave function. The amplitude of the transmitted wave function, Eq. (5), is calculated at a large distance from the end of the Coulomb barrier [35]. We carefully investigated the transmitted wave functions up to very large separation distances and found that the amplitude of the transmitted wave function reaches its fixed value at distances larger than 900 fm. In the present work, the penetration probability is obtained in terms of the amplitude of the transmitted wave function at sufficiently large distance from the end of the Coulomb barrier ($r > 1000$ fm), at which the amplitude becomes certainly constant.

Also, the knocking frequency can be defined as the inverse time for the light cluster to traverse the distance between r_1 and r_2, back and forth [27],

$$\nu = T^{-1} = \left[\int_{r_1}^{r_2} \frac{2\,\mu}{\hbar\, k(r)}\, dr \right]^{-1}. \tag{6}$$

The preformation factor S_α could be estimated from the experimental α-decay half-life time $T_\alpha^{\exp}$, and the calculated decay width ($\Gamma = \hbar\, \nu\, P$) as

$$S_\alpha = \frac{\hbar \ln 2}{\Gamma\, T_\alpha^{\exp}}. \tag{7}$$

The α-daughter interaction potential is vital in the reliable calculation of the α-decay width. In our calculations, we compute the nuclear potential microscopically by two methods. Namely, we consider the generalized double-folding model based on the realistic density-dependent M3Y-Paris nucleon-nucleon (NN) interaction [36] with a finite-range exchange part, and the Skyrme energy density formalism using the Skyrme-SLy4 effective NN interaction [9]. These trustworthy potentials are well known for their successful applications to structure and reaction studies of heavy and superheavy nuclei. The generalized double-folding nuclear potential with an explicit treatment of the isospin dependence reads

$$V_N(r) = V_0^{\rm D} + V_0^{\rm Ex} + V_1^{\rm D} + V_1^{\rm Ex}. \tag{8}$$

The isoscalar and isovector components of the direct (D) and exchange (Ex) parts of the nucleus-nucleus potential are given by [50]

$$\begin{aligned}
V_0^{\rm D}(r,E) &= \int d\vec{r}_1 \int d\vec{r}_2\, \rho_1(\vec{r}_1)\, \upsilon_{00}^{\rm D}(\rho,E,s)\, \rho_2(\vec{r}_2),\\
V_0^{\rm Ex}(r,E) &= \int d\vec{r}_1 \int d\vec{r}_2\, \rho_1(\vec{r}_1,\vec{r}_1+\vec{s})\, \rho_2(\vec{r}_2,\vec{r}_2-\vec{s})\\
&\quad \times \upsilon_{00}^{\rm Ex}(\rho,E,s) \exp\left[\frac{i\,\vec{k}(r)\cdot\vec{s}}{M}\right],\\
V_1^{\rm D}(r,E) &= \int d\vec{r}_1 \int d\vec{r}_2\, [\rho_{n1}(\vec{r}_1) - \rho_{p1}(\vec{r}_1)]\\
&\quad \times [\rho_{n2}(\vec{r}_2) - \rho_{p2}(\vec{r}_2)] \upsilon_{01}^{\rm D}(\rho,E,s),\\
V_1^{\rm Ex}(r,E) &= \int d\vec{r}_1 \int d\vec{r}_2\, \upsilon_{01}^{\rm Ex}(\rho,E,s)\, \exp\left[\frac{i\,\vec{k}(r)\cdot\vec{s}}{M}\right]\\
&\quad \times [\rho_{n1}(\vec{r}_1,\vec{r}_1+\vec{s}) - \rho_{p1}(\vec{r}_1,\vec{r}_1+\vec{s})]\\
&\quad \times \left[\rho_{n2}(\vec{r}_2,\vec{r}_2-\vec{s}) - \rho_{p2}(\vec{r}_2,\vec{r}_2-\vec{s})\right].
\end{aligned} \tag{9}$$

While $\rho_{(i=p,n)(j=1,2)}(\vec{x},\vec{x'})$ are the neutron and proton density distributions of the two interacting nuclei, the NN separation vector is $\vec{s} = \vec{r}_2 - \vec{r}_1 + \vec{r}$. Also, we have $\rho_{1(2)} = \rho_{n1(2)} + \rho_{p1(2)}$ and $M = A_1 A_2/(A_1 + A_2)$. The relative-motion momentum k is given by $k^2(r) = 2\,\mu\,[E_{\rm c.m.} - V_N(r) - V_C(r)]/\hbar^2$. μ defines the reduced mass of the interacting nuclei. $E_{\rm c.m.}$ represents the center-of-mass energy.

The energy- and density-dependent M3Y-Paris NN interaction is given in its CDM3Y form as [50]

$$\begin{aligned}
\upsilon_{00(01)}^{\rm D(EX)}(\rho,E,s) &= \upsilon_{00(01)}^{\rm D(EX)}(s)\, C_{0(1)}\,[1 - 0.003\,E/A]\\
&\quad \times [1 + \alpha \exp(-\beta\rho) + \gamma\rho].
\end{aligned} \tag{10}$$

The radial strengths of the central isoscalar ($\upsilon_{00}^{\rm D(EX)}$) and isovector ($\upsilon_{01}^{\rm D(EX)}$) direct (D) and exchange (Ex) components of the M3Y-Paris effective NN interaction were extracted from the G-matrix elements of the Paris potential [51,52]. The values of the different parameters $C_{0(1)}$, α, β, and γ are related to the equation of state of nuclear matter that described by the effective NN interaction [49]. The parameters for the density-independent M3Y-Paris NN interaction are $C_{0(1)} = 1.0$, $\alpha = \beta = \gamma = 0$. For the density-dependent CDM3Y-230 Paris NN interaction, we have $C = 0.2961$, $\alpha = 3.4171$, $\beta = 2.2333$ fm^3, and $\gamma = 2.1501$ fm^3. C_1 is usually scaled to C_0 by

a scaling factor [53]. E/A represents the incident energy per nucleon.

The folding Coulomb potential can be calculated in terms of the pp Coulomb interaction ($\upsilon_C = e^2/s$) [54],

$$V_C(r) = \iint \rho_{p\alpha}(\vec{r}_1)\,\frac{1}{|\vec{r}+\vec{r}_2-\vec{r}_1|}\,\rho_{pd}(\vec{r}_2)d\vec{r}_1 d\vec{r}_2. \quad (11)$$

The proton distributions of the α-particle ($\rho_{p\alpha}$) and the daughter nucleus (ρ_{pd}) are normalized to $2\,e$ and $Z_d\,e$, respectively.

Another realistic method we will consider here to calculate the potential is that based on the Skyrme energy density functional [9,55,56]. In this method, the nuclear interaction potential is defined as the difference between the energy expectation value E of the whole system calculated at a finite separation distance r and that calculated at infinity,

$$\begin{aligned} V_N(r) &= E(r) - E(\infty) \\ &= \int \mathcal{H}(\boldsymbol{r})d\boldsymbol{r} - \left[\int \mathcal{H}_1(\boldsymbol{r}_1)d\boldsymbol{r}_1 + \int \mathcal{H}_2(\boldsymbol{r}_2)d\boldsymbol{r}_2\right]. \end{aligned} \quad (12)$$

Here, $E(\infty)$ represents the binding energy of the nucleus and $\mathcal{H}(\boldsymbol{r})$ is the energy density functional of the Skyrme interaction [57]. In this work, we use the Skyrme force with the SLy4 parametrization [58]. The Skyrme-SLy4 NN interaction effectively describes the nuclear matter and nuclear structure properties [59–63]. It is broadly used in studying nuclear reactions of heavy nuclei [55,64–66] and their decays [9,56,67,68], as well as in investigating core-collapse supernova [69,70].

We recently improved the folding potential [36] by considering a physical internal repulsive core due to the change in the intrinsic kinetic energy of the interacting nuclei. This enhances the use of the double-folding potential in describing the reactions and decays involving large density overlap. After adding the kinetic energy term to the nuclear, Coulomb, and centrifugal parts of the interaction potential, the total potential becomes

$$V_T^K(r) = \lambda\, E_K(r) + V_N(r) + V_C(r) + \frac{\ell(\ell+1)\hbar^2}{2\mu r^2}. \quad (13)$$

The folding potential improved by considering a repulsive core of different forms has been successfully used to study the fusion reactions, electromagnetic transitions, and decays of heavy nuclei [36,47,48,71–73]. More details regarding the method of calculating the interaction potential in the framework of the double-folding model and the Skyrme energy density functional can be found in Refs. [9,36,50,54,74].

III. RESULTS AND DISCUSSION

To achieve a successful description of α decay, it is necessary to use an appropriate potential model for the α-core interaction. We consider the α-decay process for the even (Z)–even (N) and even-odd $^{105-109}$Te and $^{186,190,191,194-199,200-202,204-208,210,212-216,218,219}$Po radioactive nuclei, and for the odd-even and odd-odd $^{204,207,209,211,213-219}$At isotopes. The half-life calculations are microscopically performed in terms of the obtained wave function of the binary α-core system. Two types of realistic potentials are considered. The first type is characterized by a shallow core where no internal pocket is formed, while the second type possesses an internal pocket in its internal region. We investigate the method of applying the Bohr-Sommerfeld (BS) quantization condition to normalize the different considered potentials, either with or without using the WT rule.

We start with the α-decay process of the $^{105-109}$Te isotopes. Such nuclei with $N \approx Z$ are usually used to study the neutron-proton correlation [75,76]. Shown in Fig. 1(a) is the total interaction potential for the (α, ^{101}Sn) system, which is involved in the α decay of the ^{105}Te isotope ($Q_\alpha = 5.069$ MeV). In Fig. 1(a), the nuclear potential part is calculated based on the density-independent M3Y-Paris force and on its density-dependent CDM3Y-230 form. Figure 1(a) shows that the M3Y-Paris NN interaction yields deeper total potential in the internal interaction region, compared with the CDM3Y-230 form. Also, the density-dependent CDM3Y-230 interaction slightly lowers the Coulomb barrier height. Without adding the modified centrifugal potential, this kind of potential will not show an internal pocket. So, the correct description of the BS quantization condition to a quasibound state will not be reached. We added in Fig. 1(a) the normalized potentials after adding V_ℓ (Langer) and using the BS condition along with WT rule ($G = 16$, $n = 8$). Artificial internal pockets are then appeared for the normalized potentials in Fig. 1(a). Figure 1(b) shows the $\alpha + ^{101}$Sn total interaction potential based on the Skyrme-SLy4 interaction, with and without normalization. Added in the same figure is the folding potential based on the density-dependent CDM3Y-230 Paris interaction, which is improved by considering the repulsive intrinsic kinetic energy. The Skyrme nuclear part of the potential and the kinetic energy part of the improved folding potential are both normalized using the BS quantization condition. These two potentials are characterized by a repulsive core and a physical internal deep pocket.

Once we obtain the normalized total potential for the α-core system, we implement it in the Schrödinger wave equation. We apply the BS quantization condition once more to obtain the correct wave function for the α-core system. Figures 2(a) and 2(b) show the solution of the real part of the radial wave function for the (α, ^{101}Sn) system, based on the normalized M3Y-Paris potential and on its density-dependent CDM3Y-230 form, respectively. The normalized potentials are shown in the corresponding panels. For these types of potentials that have no physical internal pocket, the effect of the Pauli exclusion principle is taken into account by the WT rule [38]. Because we used the same normalization (λ) obtained in terms of the quantum numbers from the WT rule ($G = 16$, $n = 8$), the interior real part of the obtained wave functions exhibits eight nodes for the (α, ^{101}Sn) system, as shown in Figs. 2(a) and 2(b). The experimental half-life of ^{105}Te [77] along with the assault frequency and the penetration probability, obtained using the wave functions based on the M3Y-Paris and CDM3Y-230 potentials, yield spectroscopic factors S_α [Eq. (7)] of 0.016 and 0.005, respectively. The estimated value of S_α(M3Y) is larger than S_α (CDM3Y-230) in most cases. This is expected since the obtained Coulomb

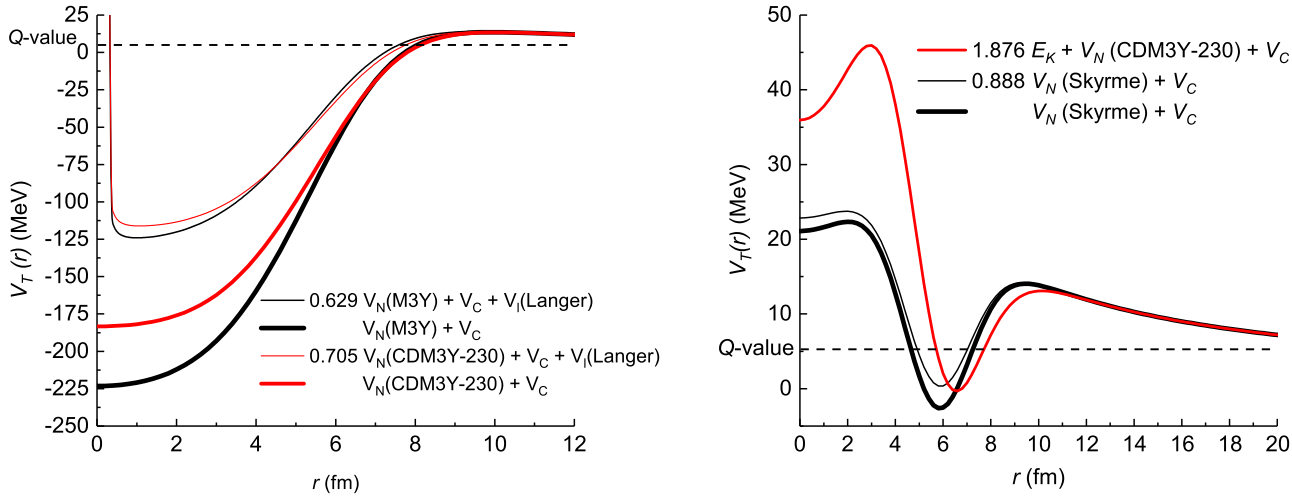

FIG. 1. The separation distance variation of the $\alpha + {}^{101}$Sn total interaction potential in the framework of (a) the double-folding model, based on the density-independent M3Y-Paris *NN* interaction and its CDM3Y-230-Paris density-dependent form, with and without normalization using the BS + WT quantization conditions after adding Langer centrifugal part, and (b) the total potential based on the improved double-folding potential based on the CDM3Y-230-Paris interaction with the repulsive intrinsic kinetic energy that is normalized using the BS quantization, and the potential based on the Skyrme-SLy4 force in the framework of the energy density formalism, with and without BS normalization.

barrier based on the M3Y-Paris interaction is wider and has larger height than that based on the density-dependent CDM3Y-230 one. On the other hand, the internal pocket obtained based on the former interaction is deeper and a bit narrower. This decreases the penetration probability and slightly increases the assault frequency based on the M3Y interaction. In most cases, this yields larger spectroscopic factor compared with that based on the density-dependent CDM3Y-230 force. For the total interaction potential based on the Skyrme energy-density formalism, which is distinguished by a physical internal pocket even without normalization, we obtained nodeless interior wave function for the (α, ^{101}Sn) system, as shown in Fig. 2(c). In a similar way, the calculations based on the improved folding potential [Fig. 1(b)] also produced nodeless wave function, as depicted in Fig. 2(d). The BS quantization condition with $n = 0$ has been used to normalize both the nuclear Skyrme potential and the kinetic energy part of the improved folding potential. The calculations performed using the wave functions based on the Skyrme-SLy4 potential and on the improved folding potential yielded spectroscopic factor values of 0.022 and 0.004, respectively.

However, when we apply the BS quantization condition for the potentials that have no internal pocket, we obtain a large number of nodes compared with the potentials characterized with a physical internal pocket. This is because the depth of the first type of potentials has to be adjusted through a convenient large quantum number for the lowest relative motion state to satisfy the Pauli exclusion principle. This takes place using the WT recipe that links the harmonic-oscillator cluster model and the harmonic oscillator shell model [38,78]. On the other hand, the repulsive part due to considering the change of the intrinsic kinetic energy for the potentials that characterized by an internal pocket effectively simulates the Pauli principle. This automatically takes into account the structure forbiddenness impacts [79] on the formed α cluster, not to move toward the center of the core nucleus. In this case, satisfying the Pauli principle using a large quantum number based on the WT prescription is obviously an improper repetition. Using the WT rule in this case yields extreme unphysical values of the normalization factor, to repeal the kinetic energy part.

For the ground-state to ground-state α decays of the $^{105-109}$Te isotopes, we display in Fig. 3 the spectroscopic preformation factor S_α as extracted using Eq. (7). The BS quantization condition is applied to normalize the different considered potentials, with different global quantum numbers. The wave functions obtained upon the different normalizations of the considered potentials possess numbers of nodes ranging from $n = 3$ to $n = 11$, which is greater than the number given by the WT prescription ($G = 16$, $n = 8$). We show in Figs. 3(a) and 3(b) the calculations based on the M3Y-Paris *NN* interaction and on its density-dependent CDM3Y-230 form, respectively. The calculations performed using the Skyrme-SLy4 potential and using the improved folding potential are displayed in Figs. 3(c) and 3(d), respectively.

Figures 3(a) and 3(b) show that the calculations based on the M3Y force and on its density-dependent form, with applying the BS quantization along with the WT rule, yield S_α of the order of 10^{-1} to 10^{-3}. Applying the BS quantization with different quantum number values starting from $n = 3$ and up to $n > n_{WT}$ yield S_α of the same orders. n_{WT} is the nodes number obtained from the WT rule. For these potentials, λ approaches unity for the large number of nodes ($n \approx 11$) and decreases with decreasing n. Increasing λ increases the attractive nuclear part of the potential. Thus, the penetration probability increases with increasing both λ and the number of nodes, upon decreasing the width of the Coulomb barrier ($r_3 - r_2$) and lowering its height. Also, the assault

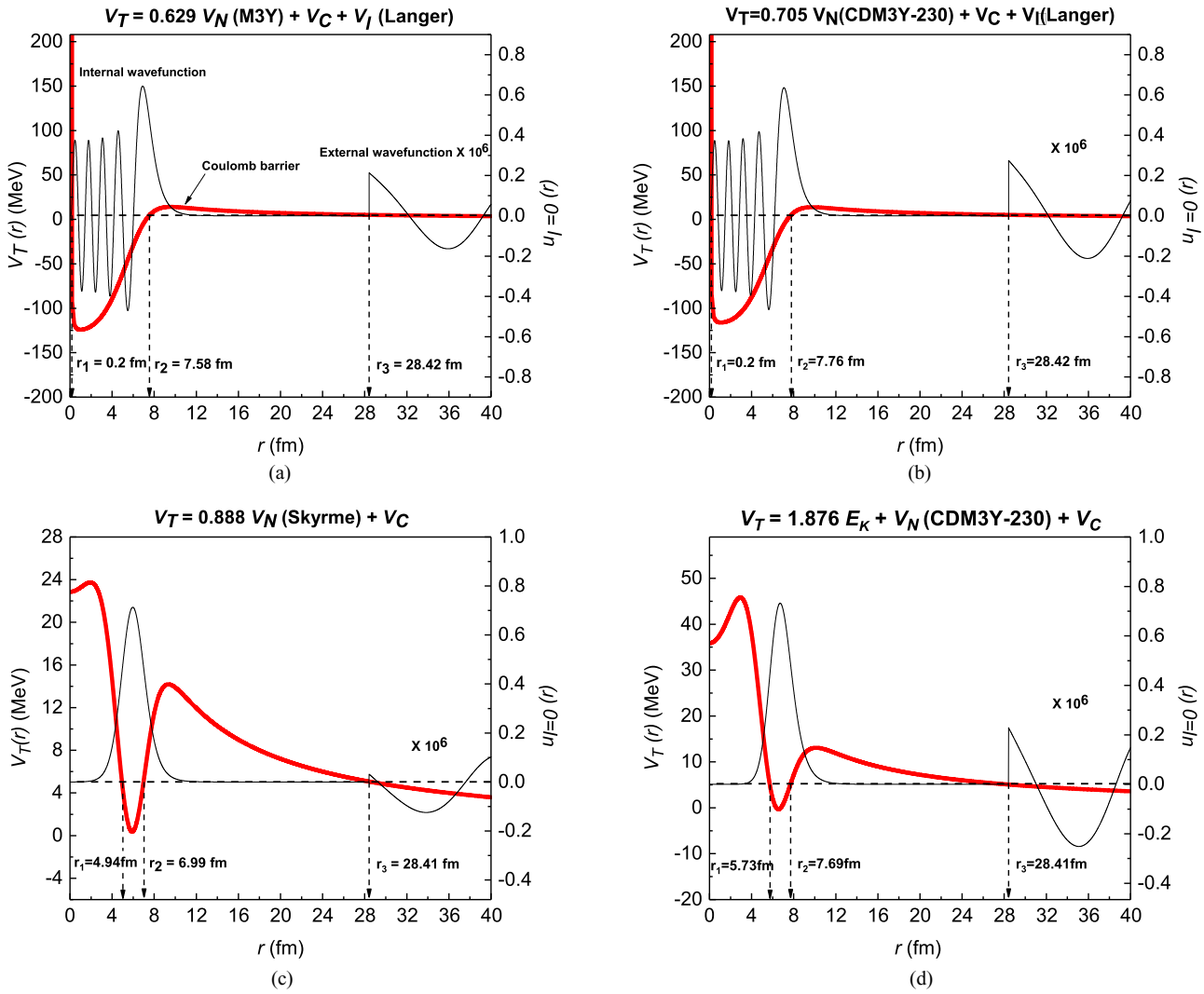

FIG. 2. The internal and external (magnified by 10^6) real part of the quasibound wave function $u_l = 0$ as obtained by solving the time-independent Schrödinger equation of the ^{105}Te ($\alpha + {}^{101}$Sn, $E = Q_\alpha = 5.069$ MeV [87]) system in its ground state based on (a) the density-independent M3Y-Paris and (b) the density-dependent CDM3Y-230-Paris, which are normalized using the BS + WT quantization conditions, and (c) the Skyrme-SLy4 force and (d) the improved folding potential in terms of the CDM3Y-230-Paris interaction plus normalized intrinsic kinetic energy (E_K), which are normalized using the BS quantization condition. The potentials are shown by the red lines.

frequency slightly increases due to increasing the depth of the internal pocket, even with increasing its width ($r_2 - r_1$). Consequently, the estimated spectroscopic factor [Eq. (7)] decreases with increasing number of nodes, upon increasing the decay width. This systematic behavior of S_α (M3Y) and S_α (CDM3Y-230) with n is clearly appear in Figs. 3(a) and 3(b), respectively. A precaution which should be mentioned here is that calculating the amplitude of the transmitted wave function at a shorter distance from the third turning point and before reaching its constant value may lead to a deviation of some estimated values of S_α from its anticipated systematic behavior with n. This is because the obtained transmitted wave function and its amplitude are correlated with the internal wave function, where they are normalized together. Hence, not only the characteristic properties of the Coulomb barrier but also the depth and width of the internal pocket of the potential influence the transmitted wave function and its amplitude, which is used to find the penetration probability. However, the different extracted values of $S_\alpha (n = 3$ to $n_{WT})$ are in good agreement with those obtained in other studies based on different models [75,76,80,81], as shown in Figs. 3(a) and 3(b). The calculations based on $n > n_{WT}$ indicate somewhat smaller values of S_α. On the other hand, the calculations based on the M3Y-Paris and the CDM3Y-230 potentials with $n \leqslant 2$ yield unrealistic values of $S_\alpha > 1$, due to the disturbing reduction of the nuclear part of the potential with $\lambda \leqslant 0.22$. It is then possible to calculate precisely the decay half-life using the potentials that have no automatic internal pocket by applying the BS quantization even with smaller quantum numbers than that obtained from the WT rule.

Regarding the nuclear potentials characterized with an automatic internal pocket, the calculations based on such potentials yield convenient values of S_α, upon applying the BS quantization with $n \leqslant 3$ for the Skyrme-SLy4 potential

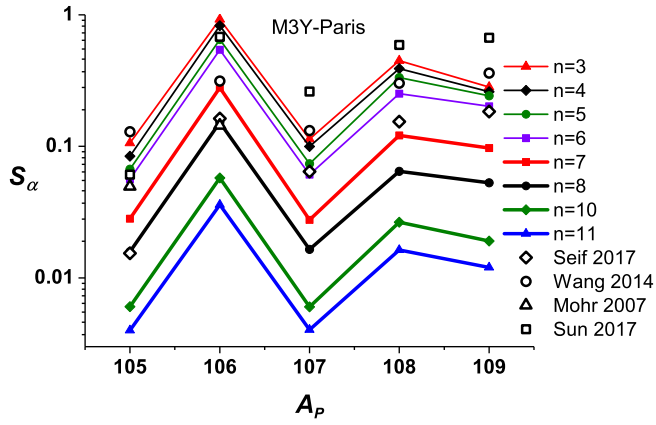

(a)

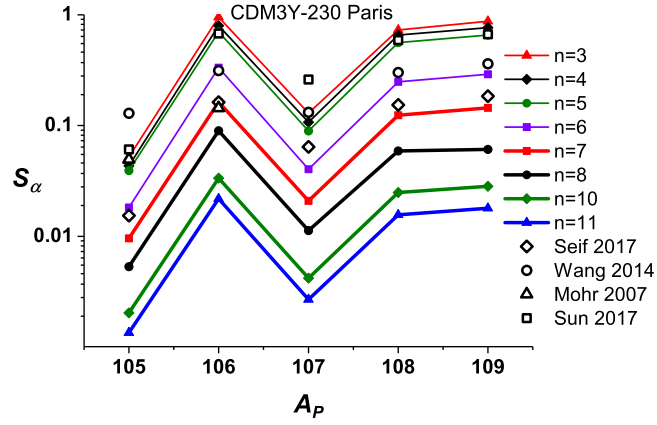

(b)

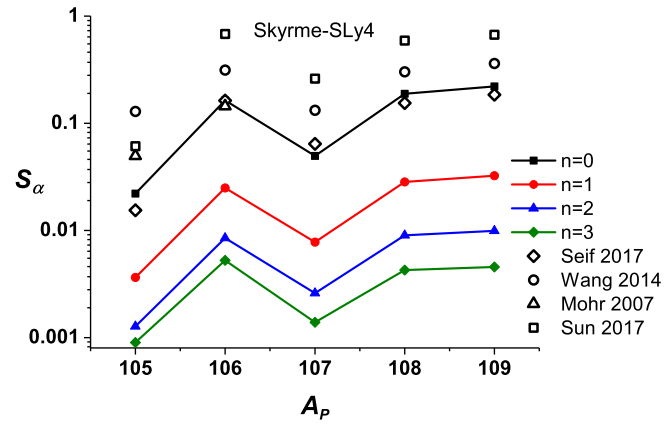

(c)

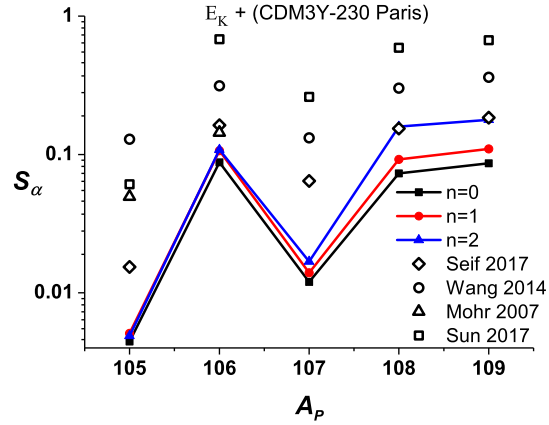

(d)

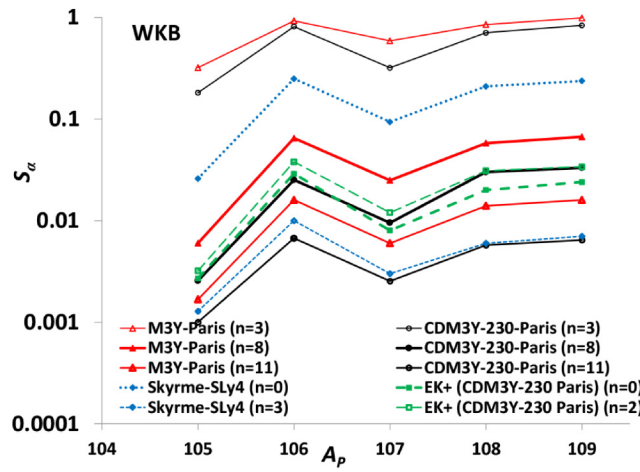

(e)

FIG. 3. The spectroscopic preformation factor of the ground-state to ground-state α decays of the $^{105-109}$Te isotopes, on a logarithmic scale, as estimated using Eq. (7) from the experimental half-life [77], and the assault frequency and penetration probability that microscopically calculated in terms of the wave functions obtained using the normalized α-daughter interaction potential based on (a) the density-independent M3Y-Paris, (b) the density-dependent CDM3Y-230-Paris, (c) the Skyrme-SLy4 force, and (d) the improved folding potential in terms of the CDM3Y-230-Paris interaction plus intrinsic kinetic energy, against the mass number of parent nuclei. Different numbers of nodes (n) are considered to normalize each examined potential using the BS quantization condition. Results from previous studies, Seif 2017 [75], Wang 2014 [76], Mohr 2007 [80], and Sun 2017 [81], based on different models, are added for comparison. (e) S_α based on the different potentials considered in panels (a)–(d), with the minimum and maximum numbers of nodes considered for these potentials as well as with $n = n_{WT}$ for the M3Y and CDM3Y-230 potentials, but the penetration probability is calculated using the WKB approximation.

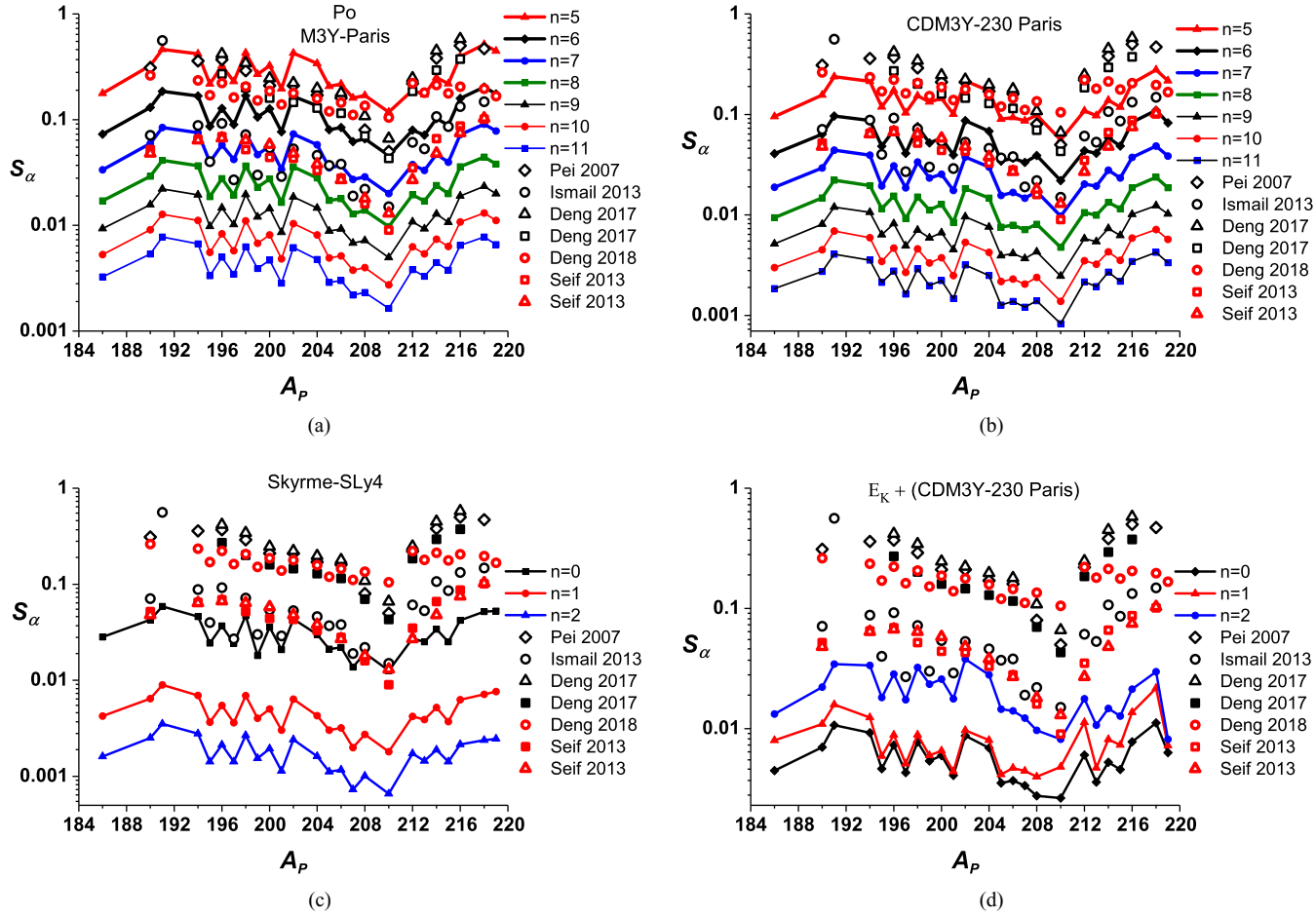

FIG. 4. Same as Fig. 3, but for the even-even and even-odd $^{186,190,191,194-199,200-202,204-208,210,212-216,218,219}$Po α emitters. Results from previous studies, Seif 2013 [56], Pei 2007 [82], Ismail 2013 [83], Deng 2017 [84], and Deng 2018 [85], based on different models, are added for comparison.

[Fig. 3(c)] and with $n \leqslant 2$ for the improved folding potential [Figs. 3(d)]. For $n = 0$, the normalization factor is ranged between 0.888 and 0.943 for the potential based on the Skyrme-SLy4 interaction. λ increases upon increasing n. The larger values of n imply extremely large values of $\lambda > 2$. With such large values of λ, the bottom of the internal pocket becomes above the Q_α value, and then no first turning point is obtained. For the calculations based on the Skyrme-SLy4 (E_K+CDM3Y-230 Paris) potential, the calculations based on $n = 0$ ($n = 2$) wave functions yield the most consistent values of S_α, compared with that obtained in previous studies [75,76,80,81].

To confirm our conclusions from Figs. 3(a)–3(d), we show in Fig. 3(e) the calculations based on the different potentials considered in Figs. 3(a)–3(d), but with the penetration probability is calculated using the Wentzel-Kramers-Brillouin (WKB) method [27,28,67] instead of using the ratio between the squared amplitudes [Eq. (5)]. In Fig. 3(e), we show the calculation based on the minimum and maximum number of nodes considered in the calculations displayed in Figs. 3(a)–3(d), for each potential. Also the calculations based on $n = n_{WT}$ for the M3Y and CDM3Y-230 potentials are presented in Fig. 3(e). Comparing Fig. 3(e) with the corresponding curves in Figs. 3(a)–3(d), one sees that the estimated preformation factors based on the two methods used to calculate penetration probability manifest typical orders of magnitude and display similar behavior patterns with n. This confirms that we can successfully reproduce the observed half-lives via applying the BS quantization condition with significantly smaller quantum numbers than that obtained from the WT prescription, even based on the potentials of no automatic internal pocket.

Regarding the favorite ground-state to ground-state α decays of the heavy even-even and even-odd $^{186,190,191,194-199,200-202,204-208,210,212-216,218,219}$Po isotopes, Fig. 4 shows the spectroscopic factor estimated from the experimental half-lives along with the calculations based on the different considered potentials. The extracted S_α for the odd-even and odd-odd $^{204,207,209,211,213-219}$At isotopes are displayed in Fig. 5. While the WT prescription estimates $G = 20$ ($n = 10$) for the α cluster inside the $^{186-210}$Po and $^{204-211}$At nuclei, it estimates $G = 22$ ($n = 11$) for the heavier isotopes of Po and At. As shown in Figs. 4(a), 4(b), 5(a), and 5(b), the calculations based on the M3Y force and on its density-dependent form and applying the BS quantization with $n = n_{WT}$ down to $n = 5$ yield S_α of the order of 10^{-1} to 10^{-3}. All these calculations reproduce

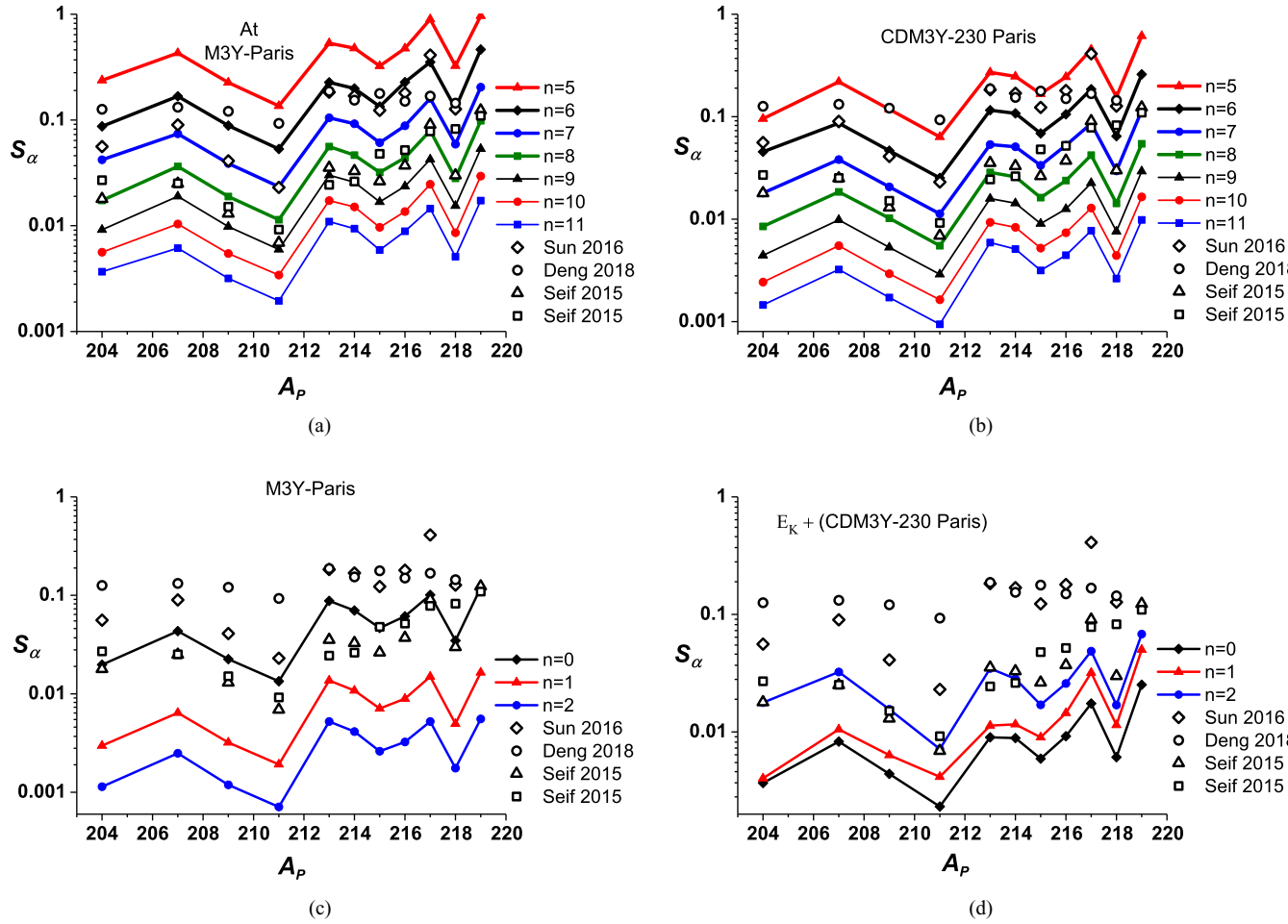

FIG. 5. Same as Fig. 3, but for the odd-even and odd-odd $^{204,207,209,211,213-219}$At α emitters. Results from previous studies, Seif 2015 [9], Deng 2018 [85], and Sun 2016 [86], based on different models, are added for comparison.

the experimental half-lives, for the two isotopic chains of Po and At, with comparable values of S_α. However, the estimated values of S_α ($n = 5$–9) show the best agreement with the values obtained in previous studies for the decays of Po [56,82–85] and At [9,85,86] nuclei, based on various models. For the density-independent M3Y-Paris interaction, the normalization factor λ for the calculations presented in Figs. 3(a), 4(a), and 5(a) upon applying the BS condition along with WT rule lies in the range of $\lambda = 0.693$–0.983. After adding the density-dependence (CDM3Y-230-Paris) in Figs. 3(b), 4(b), and 5(b), λ increases to be in the range from 0.780 to 1.098. This means that the density-dependent force expresses the *NN* interaction more appropriately than its density-independent form. In both cases, λ decreases with decreasing n, down to $\lambda(n = 3) = 0.25$ for the calculations presented in Figs. 3(a) and 3(b) and to $\lambda(n = 5) = 0.33$ for the calculations presented in Figs. 4(a), 4(b), 5(a), and 5(b). Such small values of λ weaken the role of the nuclear potential in favor of the Coulomb potential. Any further reduction of the nuclear part with smaller λ values yields unrealistic values of $S_\alpha > 1$. The conclusion that can be drawn from Figs. 3(a), 3(b), 4(a), 4(b), 5(a), and 5(b) is that we can explain the decay process using potentials with no physical internal pocket by applying the BS quantization even with quantum numbers less than those obtained from the WT prescription, down to $n_{WT} - 5$.

On the other hand, the calculations based on the Skyrme-SLy4 interaction and on the improved folding potentials give reasonable values of S_α for the considered nuclei [40,56,82–86] with $n \leqslant 2$, as seen in Figs. 4(c), 4(d), 5(c), and 5(d). Like the results obtained above for the Te isotopes, the calculations performed in terms of $n = 0$ and $n = 2$ wave functions based on the Skyrme-SLy4 and E_K+CDM3Y230 Paris potentials, respectively, yield the most consistent values of S_α, when compared with that extracted in previous studies [9,56,82–86]. Concerning the Skyme-SLy4 potentials, the normalization factor λ for the calculations presented in Figs. 3(c), 4(c), and 5(c) obtained by applying the BS condition lies in the ranges of $\lambda(n = 0) = 0.888$–1.092, $\lambda(n = 1) = 1.305$–1.506, $\lambda(n = 2) = 1.707$–1.949, and $\lambda(n = 3) = 2.053$–2.538. Here, the smaller values of λ are more credible where the large values are relatively greater than the uncertainty expected [55] in calculating the potentials based on the Skyrme interactions. The larger values of $n > 2$ ($n > 3$ for the medium-mass nuclei) require larger values of λ. This in turn rises the lowest point of the internal pocket above Q_α, and then we get no internal (first) turning point. For the improved folding potentials with the added intrinsic E_K, $\lambda(E_K)$ exhibits

the values range of $\lambda(n = 0, 1, 2) = 1.480$–$1.876$, for the calculations displayed in Figs. 3(d), 4(d), and 5(d).

IV. SUMMARY AND CONCLUSIONS

We have investigated the implementation of the Bohr-Sommerfeld quantization condition with and without the Wildermuth-Tang prescription in the microscopic α-decay calculations based on different interaction potentials. The favored ground-state to ground-state α decays of the even (Z)–even (N) and even-odd isotopes of tellurium and polonium, and the odd-even and odd-odd astatine isotopes are considered. Two types of realistic potentials for the α-daughter system have been considered, according to if they are characterized by a repulsive core or not. The adopted potentials have been normalized by applying the BS quantization condition, with and without the WT rule, and then implemented in the stationary Schrödinger equation to determine the internal and transmitted wave functions of the α-daughter system. We investigated the sensitivity of the calculated half-lives to the used potential type and to the number of nodes of the obtained wave function and its corresponding quantum numbers. We found that when we apply the BS quantization condition for the potentials that have no internal pocket we obtain interior wave function with a large number of nodes compared to the potentials characterized with an automatic internal pocket. The latter likely yield nodeless interior wave function, or of single or double nodes. This is because the former type of the potentials are normalized so as to give a depth that is chosen by appropriately large node numbers of the lowest relative motion state complying with the Pauli exclusion principle. This is given by relating the harmonic-oscillator cluster model with the harmonic-oscillator shell model through the WT rule. On the other hand, the repulsive core due to the change of the intrinsic kinetic energy in the potentials depicted by an automatic physical pocket effectively deems the Pauli principle and the structure forbiddenness influences against the movement of the formed α-cluster toward the saturated-density core. For such potentials, verifying the Pauli principle through the WT recipe is a matter of erroneous repetition. Even so, upon a proper normalization of the potential that do not exhibit subjective internal pocket, we can microscopically verify the observed half-lives by applying the BS quantization condition with significantly smaller quantum numbers than those obtained from the WT rule.

[1] N. T. Brewer, V. K. Utyonkov, K. P. Rykaczewski, Y. T. Oganessian, F. S. Abdullin, R. A. Boll, D. J. Dean, S. N. Dmitriev, J. G. Ezold, L. K. Felker *et al.*, Phys. Rev. C **98**, 024317 (2018).

[2] Y. T. Oganessian and K. P. Rykaczewski, Phys. Today **68**(8), 32 (2015).

[3] Y. T. Oganessian and V. K. Utyonkov, Rep. Prog. Phys. **78**, 036301 (2015).

[4] Y. T. Oganessian, F. S. Abdullin, P. D. Bailey, D. E. Benker, M. E. Bennett, S. N. Dmitriev, J. G. Ezold, J. H. Hamilton, R. A. Henderson, M. G. Itkis *et al.*, Phys. Rev. Lett. **104**, 142502 (2010).

[5] S. Hofmann and G. Munzenberg, Rev. Mod. Phys. **72**, 733 (2000).

[6] M. Ismail and A. Adel, J. Phys. G: Nucl. Part. Phys. **46**, 075105 (2019).

[7] W. M. Seif, N. V. Antonenko, G. G. Adamian, and H. Anwer, Phys. Rev. C **96**, 054328 (2017).

[8] D. Ni and Z. Ren, Phys. Rev. C **92**, 054322 (2015).

[9] W. M. Seif, Phys. Rev. C **91**, 014322 (2015).

[10] M. Ismail, W. M. Seif, A. Adel, and A. Abdurrahman, Nucl. Phys. A **958**, 202 (2017).

[11] M. Ismail, A. Y. Ellithi, M. M. Botros, and A. Adel, Phys. Rev. C **81**, 024602 (2010).

[12] A. N. Andreyev, M. Huyse, P. Van Duppen, J. F. C. Cocks, K. Helariutta, H. Kettunen, P. Kuusiniemi, M. Leino, W. H. Trzaska, K. Eskola, and R. Wyss, Phys. Rev. Lett. **82**, 1819 (1999).

[13] H. O. U. Fynbo, C. A. Diget, U. C. Bergmann, M. J. G. Borge, J. Cederkäll, P. Dendooven, L. M. Fraile, S. Franchoo, V. N. Fedosseev, B. R. Fulton *et al.*, Nature (London) **433**, 136 (2005).

[14] W. M. Seif, H. Anwer, and A. R. Abdulghany, Ann. Phys. **401**, 149 (2019).

[15] M. Ismail and A. Adel, Phys. Rev. C **97**, 044301 (2018).

[16] G. Gamow, Z. Physik **51**, 204 (1928)

[17] R. W. Gurney and E. U. Condon, Nature (London) **122**, 439 (1928).

[18] L. Ghys, A. N. Andreyev, M. Huyse, P. Van Duppen, S. Antalic, A. Barzakh, L. Capponi, T. E. Cocolios, J. Cubiss, X. Derkx *et al.*, Phys. Rev. C **100**, 054310 (2019).

[19] J. G. Cubiss, A. N. Andreyev, A. E. Barzakh, B. Andel, S. Antalic, T. E. Cocolios, T. D. Goodacre, D. V. Fedorov, V. N. Fedosseev, R. Ferrer *et al.*, Phys. Rev. C **99**, 064317 (2019).

[20] D. S. Delion, *Theory of Particle and Cluster Emission* (Springer-Verlag, Berlin, 2010).

[21] V. E. Viola and G. T. Seaborg, J. Inorg. Nucl. Chem. **28**, 741 (1966).

[22] G. Royer and H. F. Zhang, Phys. Rev. C **77**, 037602 (2008).

[23] Y. Ren and Z. Ren, Phys. Rev. C **85**, 044608 (2012).

[24] C. Qi, F. R. Xu, R. J. Liotta, R. Wyss, M. Y. Zhang, C. Asawatangtrakuldee, and D. Hu, Phys. Rev. C **80**, 044326 (2009).

[25] J. Dong, H. Zhang, Y. Wang, W. Zuo, and J. Li, Nucl. Phys. A **832**, 198 (2010).

[26] C. Xu and Z. Ren, Phys. Rev. C **74**, 014304 (2006).

[27] N. G. Kelkar and H. M. Castaneda, Phys. Rev. C **76**, 064605 (2007).

[28] S. A. Gurvitz and G. Kalbermann, Phys. Rev. Lett. **59**, 262 (1987).

[29] D. Ni and Z. Ren, Phys. Rev. C **81**, 064318 (2010).

[30] Y. Qian, Z. Ren, and D. Ni, J. Phys. G: Nucl. Part. Phys. **38**, 015102 (2011).

[31] M. Mirea, Phys. Rev. C **96**, 064607 (2017).

[32] V. I. Furman, S. Holan, S. G. Kadmensky, and G. Stratan, Nucl. Phys. A **226**, 131 (1974).

[33] D. S. Delion, Z. Ren, A. Dumitrescu, and D. Ni, J. Phys. G: Nucl. Part. Phys. **45**, 053001 (2018).

[34] R.-Y. Wang, Y.-B. Qian, and Z. Ren, Chin. Phys. C **41**, 064103 (2017).
[35] J. Dong, W. Zuo, and W. Scheid, Nucl. Phys. A **861**, 1 (2011).
[36] W. M. Seif, A. M. H. Abdelhady, and A. Adel, J. Phys. G: Nucl. Part. Phys. **45**, 115101 (2018).
[37] B. Buck, A. C. Merchant, and S. M. Perez, Phys. Rev. Lett. **76**, 380 (1996).
[38] K. Wildermuth and Y. C. Tang, *A Unified Theory of the Nucleus* (Academic Press, New York, 1977).
[39] D. Ni and Z. Ren, J. Phys. G: Nucl. Part. Phys. **37**, 035104 (2010).
[40] W. M. Seif, M. Shalaby, and M. F. Alrakshy, Phys. Rev. C **84**, 064608 (2011).
[41] M. Ismail and A. Adel, J. Phys. G: Nucl. Part. Phys. **44**, 125106 (2017).
[42] J. Dong, W. Zuo, J. Gu, Y. Wang, and B. Peng, Phys. Rev. C **81**, 064309 (2010).
[43] B. Buck, A. C. Merchant, S. M. Perez, and P. Tripe, Phys. Rev. C **47**, 1307 (1993).
[44] B. Buck, A. C. Merchant, M. J. Horner, and S. M. Perez, Nucl. Phys. A **673**, 157 (2000).
[45] H. F. Zhang, G. Royer, and J. Q. Li, Phys. Rev. C **84**, 027303 (2011).
[46] W. Seif, M. Ismail, A. Rafaie, and L. H. Amer, J. Phys. G: Nucl. Part. Phys. **43**, 075101 (2016).
[47] S. Peltonen, D. S. Delion, and J. Suhonen, Phys. Rev. C **75**, 054301 (2007).
[48] D. S. Delion, S. Peltonen, and J. Suhonen, Phys. Rev. C **73**, 014315 (2006).
[49] W. M. Seif, J. Phys. G **38**, 035102 (2011).
[50] D. T. Khoa, W. von Oertzen, and A. A. Ogloblin, Nucl. Phys. A **602**, 98 (1996).
[51] N. Anantaraman, H. Toki, and G. F. Bertsch, Nucl. Phys. A **398**, 269 (1983).
[52] G. Bertsch, J. Borysowicz, H. McManaus, and G. R. Satchler, Nucl. Phys. A **284**, 399 (1977).
[53] D. T. Khoa and H. S. Than, Phys. Rev. C **71**, 044601 (2005).
[54] M. Ismail, W. M. Seif, and H. El-Gebaly, Phys. Lett. B **563**, 53 (2003).
[55] W. M. Seif, Eur. Phys. J. A **38**, 85 (2008).
[56] W. M. Seif, J. Phys. G: Nucl. Part. Phys. **40**, 105102 (2013).
[57] D. Vautherin and D. M. Brink, Phys. Rev. C **5**, 626 (1972).
[58] E. Chabanat, P. Bonche, E. Haensel, J. Meyer, and R. Schaeffer, Nucl. Phys. A **635**, 231 (1998).
[59] Y. Fu, H. Tong, X. F. Wang, H. Wang, D. Q. Wang, X. Y. Wang, and J. M. Yao, Phys. Rev. C **97**, 014311 (2018).
[60] A. P. Severyukhin, S. Åberg, N. N. Arsenyev, and R. G. Nazmitdinov, Phys. Rev. C **95**, 061305(R) (2017).
[61] W. M. Seif and H. Mansour, Internat. J. Modern Phys. E **24**, 1550083 (2015).
[62] L. Bonneau, P. Quentin, and K. Sieja, Phys. Rev. C **76**, 014304 (2007).
[63] A. S. Umar and V. E. Oberacker, Phys. Rev. C **76**, 024316 (2007).
[64] R. Keser, A. S. Umar, and V. E. Oberacker, Phys. Rev. C **85**, 044606 (2012).
[65] Z.-Q. Feng, G.-M. Jin, and F.-S. Zhang, Nucl. Phys. A **802**, 91 (2008).
[66] A. S. Umar, V. E. Oberacker, and C. J. Horowitz, Phys. Rev. C **85**, 055801 (2012).
[67] W. M. Seif, M. M. Botros, and A. I. Refaie, Phys. Rev. C **92**, 044302 (2015); Indian J. Phys. **92**, 393 (2018).
[68] D. E. Ward, B. G. Carlsson, and S. Åberg, Phys. Rev. C **88**, 064316 (2013).
[69] H. Pais, W. G. Newton, and J. R. Stone, Phys. Rev. C **90**, 065802 (2014).
[70] H. Pais and J. R. Stone, Phys. Rev. Lett. **109**, 151101 (2012).
[71] Ş. Mişicu and H. Esbensen, Phys. Rev. Lett. **96**, 112701 (2006).
[72] D. S. Delion and A. Dumitrescu, Phys. Rev. C **87**, 044314 (2013).
[73] A. Dumitrescu and D. S. Delion, Phys. Rev. C **93**, 024313 (2016).
[74] M. Ismail and A. Adel, Phys. Rev. C **84**, 034610 (2011).
[75] W. M. Seif, M. Ismail, and E. T. Zeini, J. Phys. G: Nucl. Part. Phys. **44**, 055102 (2017).
[76] Y. Z. Wang, J. Z. Gu, and Z. Y. Hou, Phys. Rev. C **89**, 047301 (2014).
[77] G. Audi, F. G. Kondev, M. Wang, W. J. Huang, and S. Naimi, Chin. Phys. C **41**, 030001 (2017).
[78] R. Lovas, R. Liotta, A. Insolia, K. Varga, and D. Delion, Phys. Rep. **294**, 265 (1998).
[79] G. G. Adamian, N. V. Antonenko, N. Nenoff, and W. Scheid, Phys. Rev. C **64**, 014306 (2001).
[80] P. Mohr, Eur. Phys. J. A **31**, 23 (2007).
[81] X.-D. Sun, J.-G. Deng, D. Xiang, P. Guo, and X.-H. Li, Phys. Rev. C **95**, 044303 (2017).
[82] J. C. Pei, F. R. Xu, Z. J. Lin, and E. G. Zhao, Phys. Rev. C **76**, 044326 (2007).
[83] M. Ismail and A. Adel, Phys. Rev. C **88**, 054604 (2013).
[84] D. Deng and Z. Ren, Phys. Rev. C **96**, 064306 (2017).
[85] J.-G. Deng, J.-C. Zhao, P.-C. Chu, and X.-H. Li, Phys. Rev. C **97**, 044322 (2018).
[86] X.-D. Sun, P. Guo, and X. H. Li, Phys. Rev. C **94**, 024338 (2016).
[87] M. Wang, G. Audi, F. Kondev, W. Huang, S. Naimi, and X. Xu, Chin. Phys. C **41**, 030003 (2017).